Lagrangian Two-Phase Flow Modeling of Scour in Front of Vertical Breakwater

Abbas Yeganeh-Bakhtiary[1,2,*], Hamid Houshangi[3] and Soroush Abolfathi[4]

[1] School of Civil Engineering, Iran University of Science & Technology (IUST), Narmak, Tehran 16844, Iran, yeganeh@iust.ac.ir

[2] Department of Civil and Architectural Engineering, University of Kurdistan Hewler (UKH), Erbil 44001, Iraq, abbas.yeganeh@ukh.edu.krd

[3] Bonyan Institute of Higher Education, Shahinshahr, Isfahan, Iran, houshangi@alumni.iust.ac.ir

[4] School of Engineering, University of Warwick, Coventry, CV4 7AL, United Kingdom, Soroush.Abolfathi@warwick.ac.uk

Abstract

A Lagrangian particle-based two-phase flow model is developed to simulate the scouring process induced by standing wave in front of the trunk section of a vertical breakwater. Given the two-dimensional nature of the scouring problem at the trunk of vertical wall, the fluid phase is simulated with two-dimensional Navier–Stokes equations based on Weakly Compressible Smoothed Particle Hydrodynamics (WCSPH) formulation in conjunction with Sub-Particle Scale (SPS) turbulence closure model. The sediment phase is simulated using the Discrete Element Method (DEM). The effects of interparticle and particle-wall collisions are computed by activating a spring-dashpot system. The WCSPH fluid-phase and DEM sediment-phase are coupled through a weakly one-way coupling procedure using wave orbital velocity. The numerical model is successfully validated against experimental data. The maximum scour depth predicted by WCSPH-DEM model is closely approximate the experimental data. This study, for the first time, demonstrated an extra recirculating sediment transport mechanism in front of the vertical breakwater, similar to steady streaming recirculating cells in the fluid phase, which has a direct impact on the formation of scour hole and maximum scour depth at the breakwater trunk. The scenario modelling conducted in this study show that by increasing the steady streaming velocity, the deposition rate and the depth of scour hole were increased.

Keywords: Lagrangian Two-phase flow model, particle-based methods, WCSPH, DEM, scouring, vertical breakwater.

1 Introduction

The significance of scouring in structural stability and functionality of coastal structures, specifically vertical breakwaters, have led into many experimental [de Best & Bijker, 1971; Xie, 1981; Irie & Nadaoka, 1984; Hughes & Flower, 1991; Sumer & Fredsøe, 2002] and numerical [Chen, 2007; Gislason et al., 2009 a, b; Yeganeh-Bakhtiary et al., 2010 & 2017; Tahersima et al., 2011; Hajivalie et al., 2012; Tofani et al., 2014; Dong et al., 2018] investigations to understand the underlying hydrodynamic deriving mechanisms and scouring pattern. When the incident wave terrain reaches the vertical breakwater in shore-normal angle of approach, the scour in front of the trunk section of vertical wall-type breakwater is a two-dimensional process [Sumer & Fredsøe, 2002]. The interactions between incident waves attacking the structure and reflected waves from vertical breakwater produce a series of standing waves in front of breakwater's trunk section [Lillycrop & Hughes, 1993; Oumeraci, 1994 a & b; Sumer & Fredsøe, 2002]. The key underlying hydrodynamic mechanism of scouring is the steady streaming field, including bottom and top recirculating fluid cells at trunk section of vertical breakwater. The sediment particles behavior is profoundly affected by recirculating fluid cells; in which the fine and coarse sediments are picked up and transported by the top and bottom recirculating cells, respectively (Figure 1).

The majority of existing numerical studies, on scouring in front of vertical breakwater, are based on single-phase process-based models discretized in Eulerian formation. Simulating scouring processes with Eulerian methods is not a straightforward task, due to the challenges associated with trace of the fluid-sediment interphase momentum exchange, during the simulation. Furthermore, the process-based models are not capable of robust calculation of

distinctive aspect of sediment transport including, complicated fluid-sediment and particle-wall interactions, interparticle collisions and the momentum exchanges between the sediment and fluid.

Lagrangian particle-based flow models are robust numerical techniques, suitable for fluid–sediment interphase simulations, and capable of precise interphase computation during each time step [e.g., Potapov et al., 2001; Shao & Lo 2003; Gotoh et al., 2009; Fernandez et al., 2011; Huang & Nydal, 2012; Zanganeh et al., 2012; Wang et al., 2016; Gotoh & Khayyer, 2018; Harada et al., 2018 & 2019]. The Lagrangian modelling approaches compute particle movement for each phase based on their specific physical characteristics and therefore do not require interphase [Gotoh & Sakai, 1999; Gotoh et al., 2005; Kayyer & Gotoh, 2008; Ataie-Ashtiani & Mansour-Rezaei, 2009; Zhang et al., 2009; Zheng et al., 2017; Abolfathi et al., 2018; He et al., 2018; Khayyer et al., 2018; Wang et al., 2019].

This study develops a new Lagrange–Lagrange two-phase flow model to simulate scouring process, and describes the pertinent hydrodynamics and sediment transport processes in front of a vertical breakwater under the influence of standing wave conditions. The fluid phase is simulated by the solution of two-dimensional Navier–Stokes (N-S) equations based on WCSPH method in conjunction with the SPS turbulence closure model. The sediment phase is simulated using DEM model to determine the effects of interparticle and particle-wall collisions with activating a spring-dashpot system. The WCSPH and DEM models were coupled using the wave orbital velocity through a weakly one-way coupling procedure. The sediment transport process, scour – deposition pattern, and the momentum exchanges between fluid-sediment interphase are

systematically analyzed to understand the sediment transport dynamics and the impact of standing wave hydrodynamics on scouring patterns in front of vertical breakwaters.

2 Governing Equations

The governing equations of fluid phase include mass (Eq. 1) and momentum (Eq. 2) equations as follows:

$$\frac{1}{\rho}\frac{D\rho}{Dt} + \nabla.\vec{u} = 0 \tag{1}$$

$$\frac{D\vec{u}}{Dt} = -\frac{1}{\rho}\nabla P + \nu_0\nabla^2\vec{u} + \frac{1}{\rho}\nabla.\vec{\tau} + \vec{g} \tag{2}$$

where $\vec{u}$, ρ, P, and ν_0 are the velocity vector, density, pressure, and the kinematic viscosity ($10^{-6}\ m^2/s$) of fluid particles, respectively. ∇P denotes the pressure force, $\nu_0\nabla^2\vec{u}$ and $\nabla.\vec{\tau}$ represent the viscosity forces between fluid particles, $\vec{\tau}$ is the SPS stress tensor, and $\vec{g} = (0, -9.81)\ m/s^2$ is the gravitational acceleration vector. Eq. 1 is written in compressible form; while in the momentum equation (Eq. 2), viscosity effects is very important. The viscous effects can be simulated by artificial viscosity [Monaghan, 1992] or approximated by laminar viscosity [Morris et al., 1997]. This study adopts the Sub-Particle Scale (SPS) technique by using artificial and laminar viscosity approaches [Dalrymple & Rogers, 2006]. This study adopted the Sub-Particle Scale (SPS) turbulence model [Gotoh et al., 2001] by using artificial and the laminar viscosity approaches [Dalrymple & Rogers, 2006]. The SPS closure model performs robustly for simulation of standing wave interaction with vertical breakwater, until the PS turbulence quantity effect is negligible [Yeganeh-Bakhtiary et al., 2017]. The eddy viscosity assumption based on the Boussinesq's hypothesis is adopted to simulate the SPS stress tensor (τ_{ij}):

$$\tau_{ij} = \rho\left(2\nu_t S_{ij} - \frac{2}{3}k_{SPS}\delta_{ij}\right) - \frac{2}{3}\rho C_I \Delta^2 \delta_{ij}\left|S_{ij}\right|^2 \quad (3)$$

where C_I is a constant set to 0.0066 according to Blinn et al. [2002], k_{SPS} is the SPS turbulence kinetic energy, Δ is the initial particle-particle spacing, S_{ij} is the element of SPS strain-rate tensor, ν_t is the turbulent eddy viscosity, and δ_{ij} is Kronecker delta. The standard Smagorinsky model was applied to determine the turbulent eddy viscosity [Smagorinsky, 1963; Gotoh et al., 2004; Shao & Gotoh, 2004]

$$\nu_t = (\mathrm{C_s}\Delta)^2|S| \quad (4)$$

here $C_s = 0.12$ is the Smagorinsky constant and $|S| = \left(2S_{ij}S_{ij}\right)^{1/2}$ is the local strain rate.

The governing equations for sediment particles based on Newton laws could be written as

$$m_i \frac{d\vec{u}_i}{dt} = \sum_j \vec{F}_{c,ij} + \vec{F}_{fs,i} + m_i\vec{g} \quad (5)$$

$$I_i \frac{d\vec{\omega}_i}{dt} = -\sum_j R_i \vec{n}_{ij} \times \vec{F}_{c,ij} \quad (6)$$

$$\frac{d\vec{r}_i}{dt} = \vec{u}_i \quad (7)$$

where subscripts i and j are for identifying particles, m is the mass, $\vec{u}$ is the velocity of the center of mass, , $\vec{\omega}$ is the angular velocity, $\vec{r}$ denotes the particle position, R is the particle radius, $\vec{F}_{c,ij}$ is the contact force of particle j acting on i, $\vec{F}_{fs,i}$ is the fluid–sediment interaction force which is assumed to act at the center of mass of particles, I_i is the inertia moment of a sediment particle, and $\vec{n}_{ij}$ is the normal direction of the contact pointing to particle i from j.

3 Numerical Model

3.1 WCSPH Model

WCSPH technique is employed to simulate the fluid phase [Monaghan, 1992]. Eqs. 8 and 9 present the WCSPH formulation for mass [Monaghan, 1992] and momentum [Dalrymple & Rogers, 2006] conservation, respectively.

$$\frac{d\rho_a}{dt} = \sum_b m_b \vec{u}_{ab} \vec{\nabla}_{\mathrm{a}} W_{ab} \tag{8}$$

$$\begin{aligned} \frac{d\vec{u}_a}{dt} = &- \sum_b m_b \left(\frac{P_a}{\rho_a^2} + \frac{P_b}{\rho_b^2}\right) \vec{\nabla}_{\mathrm{a}} W_{ab} + \sum_b m_b \left(\frac{4\nu_0 \vec{r}_{ab} \vec{u}_{ab}}{(\rho_a + \rho_b)(|\vec{r}_{ab}|^2 + \lambda^2)}\right) \vec{\nabla}_{\mathrm{a}} W_{ab} \\ &+ \sum_b m_b \left(\frac{\tau_a}{\rho_a^2} + \frac{\tau_b}{\rho_b^2}\right) \vec{\nabla}_{\mathrm{a}} W_{ab} + \vec{g} \end{aligned} \tag{9}$$

where W_{ab} is kernel function varying from 0 to 1 [Monaghan & Lattanzio, 1985], a and b are the reference particle and its neighbors; $\vec{u}_{ab} = \vec{u}_a - \vec{u}_b$, $\vec{r}_{ab} = \vec{r}_a - \vec{r}_b$, λ is a small number introduced to keep the denominator non-zero (=$0.1h_{ab}$).

The WCSPH model adopts equation of state (Eq. 10) to approximate the pressure field.

$$P = B\left[\left(\frac{\rho}{\rho_0}\right)^{\gamma} - 1\right] \tag{10}$$

here γ is a constant (=7), ρ_0 is the reference density (=1000kg/m^3) and constant B controls the relative density fluctuation $\frac{|\Delta\rho|}{\rho_0}$, with $\Delta\rho = \rho - \rho_0$.

The fluid model uses XSPH equation (Eq. 11) to compute the particles movements [Monaghan, 1994], and ensures smooth distribution of velocity between the neighboring particles.

$$\left(\frac{d\vec{r}}{dt}\right)_a = \vec{u}_a + \varepsilon \sum_b \frac{m_b}{\bar{\rho}_{ab}} (\vec{u}_b - \vec{u}_a) W_{ab} \tag{11}$$

where ε is a constant (=0.5) and $\bar{\rho}_{ab} = (\rho_a + \rho_b)/2$.

A Predictor-Corrector time marching scheme of second order accuracy [Monaghan, 1995] was employed to solve the N-S equations for the fluid phase. At the first stage, values of velocity, density and position at $t^{n+1/2}$ are predicted from values at t^n and $t^{n-1/2}$. Then, force and other variables are computed based on these predicted values. At the second stage, field variables at $t^{n+1/2}$ are corrected using the new values. Finally, all variables at t^{n+1} are obtained using the trapezoidal rule.

The density (Eq. 8) and pressure (Eq. 10) of particles increase as they approach wall boundaries due to the pressure term in momentum equation. This results in the repulsion of the particles within the distance of $2h$ from the wall. A dynamic boundary condition was adopted in which the boundary particles are forced to satisfy the same equations as the fluid particles [Crespo et al., 2007]. Although after each time-step the boundary particles remained fixed in their initial positions.

3.2 DEM Model

The sediment phase is simulated using two-dimensional form of the Movable Bed Simulator (MBS-3D) model developed by Yeganeh-Bakhtiary et al. [2009]. The sediment model uses Cundall & Strack [1979] idea for discrete regions where small deformations and multiple contacts on a particle are computed with considering both friction and rotation. In the present study, the DEM calculation is formulated with the assumption of spherical shape for sediment particles of the same diameter. A spring-dashpot model is activated to simulate the collision effects between particles, and signify elastic-damping forces. If the distance between the centers of mass of two particles exceed their diameters, the collision force between them is assumed to be zero. Otherwise, they are in contact if $\left[(x_i - x_j)^2 + (y_i - y_j)^2\right]^{1/2} < 2\varphi R$; here (x_i, y_i) and (x_j, y_j) are the coordinate of central point of the i^{th} and j^{th} particles, and φ is a constant ($\cong$1.0).

The DEM model uses a local coordinate (ξ, η) for sediment particles in addition to global coordinate (x, y). The collision force acting on solid particle i from particle $j, \vec{F}_{j\to i} = \left(F_{j\to i}^{\xi}, F_{j\to i}^{\eta}\right)$, is determined with Eq. 12 [Yeganeh-Bakhtiary et al., 2009].

$$\begin{cases} F_{j\to i}^{\xi}(t) = e_n(t) + d_n(t) \\ F_{j\to i}^{\eta}(t) = e_s(t) + d_s(t) \end{cases} \tag{12}$$

where ξ and η are the local coordinates in normal and tangential directions respectively, e denotes the elastic forces, d is the damping forces and subscript *n* and *s* respectively represent the normal and tangent directions. Elastic and damping forces in normal and tangent directions are computed according to Eq. 13:

$$e_n(t) = e_n(t - \Delta t_{DEM}) + k_n \Delta \xi_{i,j}; \qquad d_n(t) = c_n \frac{\Delta \xi_{i,j}}{\Delta t_{DEM}}$$
$$e_s(t) = e_s(t - \Delta t_{DEM}) + k_s \Delta \eta_{i,j}; \qquad d_s(t) = c_s \frac{\Delta \eta_{i,j}}{\Delta t_{DEM}} \tag{13}$$

here $\Delta \xi_{i,j}$, $\Delta \eta_{i,j}$ are the displacement of sediment particles during the time step of the calculation Δt_{DEM}; k_n, k_s are the spring constants. DEM model was developed with the assumption of non-cohesive sediment grains, hence the resistance against tension forces were not considered for joint between contacting particles. A shear stress limit was utilized in the local tangential direction, where the joint slips by exceeding this limit. The joint characteristics and the collision force are described in the following equations:

$$F^{\xi}_{j \to i}(t) = F^{\eta}_{j \to i}(t) = 0 \quad \text{if} \quad e_n(t) \leq 0 \tag{14}$$

$$\left| F^{\xi}_{j \to i}(t) \right| = \mu |e_n(t)| \quad \text{if} \ |e_n(t)| > \mu e_n(t) \tag{15}$$

where $\mu = 0.55$ is the maximum static friction coefficient. According to Eq. 14 no contact effect was computed for negative elastic force. Eq. 15 introduces a switch mechanism between static and dynamic friction forces. The time step Δt_{DEM} was set proportional to critical time step Δt_c to satisfy the DEM model stability. For a single mass-spring system with a degree of freedom based on the mass m, Δt_{DEM} and Δt_c are determined as:

$$\Delta t_{DEM} = \frac{\Delta t_c}{20}; \quad \Delta t_c = 2\pi \sqrt{\frac{m}{2k_n}}; \quad k_n = \frac{m}{2}\left(\frac{2\pi}{\Delta t_c}\right)^2 \tag{16}$$

In the present model, the time step is considered as $\Delta t_{DEM} = 4.5 \times 10^{-6}\ sec$; k_n, k_s, c_n and c_s were determined according to Eq. 16 and the theory of elasticity (Eq. 17).

$$k_s = \frac{k_n}{2(1+\upsilon)}; \quad c_s = \frac{c_n}{\sqrt{2(1+\upsilon)}}; \quad c_n = \alpha_{cn}.2\sqrt{mk_n} \tag{17}$$

here υ is the Poisson's ratio (=0.3) and α_{cn} is a calibrating coefficient taken as 1 [Yeganeh-Bakhtiary et al., 2009].

The total collision force acting on particle i is computed as summation of all forces applied by the neighboring particles that are in contact with particle i (Eq. 18).

$$\vec{F}_{c,i} = \sum_j \vec{F}_{j\to i} \tag{18}$$

3.3 Fluid-Sediment Coupling

The coupled WCSPH-DEM model was developed with considering the drag, lift, added mass, and buoyancy as the interaction forces between the fluid and sediment phases. A weakly one-way WCSPH-DEM coupled model was developed to apply the interphase interaction forces. B-spline kernel function with a characteristic width of *h* (the smoothing length) was applied over all fluid particles in the vicinity of each sediment particle, to determine the interaction forces within the smoothing kernel. For sediment particle in DEM model, only the forces driven from the fluid particles' movement were considered. Thus, the interaction forces of fluid particles within influence domain of a sediment particle were determined using an appropriate kernel function with smooth length according to diameter of the sediment particle. Figure 2 illustrates the schematic of interaction between fluid and sediment particles.

The coupling technique used for this study, first launch the fluid dynamic solver (WCSPH model) individually, then the results of the fluid phase were imported to the DEM model, in

which the fluid impacts on sediment particles were computed. The full coupling approach is time-consuming and challenging to converge. However, the weakly one-way coupling technique presented in this study, is computationally robust and efficient, given that the fluid particles at the upper part of the water column are not considerably influenced by the presence of sediment particles. Additionally, inside the hyper-concentrated layer of moving sediments, the velocity gradient between the fluid and sediment particles can be neglected [Hajivalie et al., 2012; Yeganeh-Bakhtiary et al., 2009].

The equations of motion (Eqs. 5 & 6) for the i^{th} particle, considering interaction forces between fluid and sediment particles in two dimensional coordinates, are computed as follow:

$$\rho\left(\frac{\rho_s}{\rho}+C_M\right)A_3D_i^3\left(\frac{du_s}{dt}\right)_i$$

$$=\sum_j F_{c,j\to i}^x+\frac{\rho}{2}C_DA_2D_i^2\sqrt{\left(u_f-u_{s,i}\right)^2+\left(w_f-w_{s,i}\right)^2}\left(u_f-u_{s,i}\right) \tag{19}$$

$$+\frac{\rho}{2}C_LA_2D_i^2\left|w_f-w_{s,i}\right|\frac{\partial\left(u_f-u_{s,i}\right)}{\partial z}$$

$$\rho\left(\frac{\rho_s}{\rho}+C_M\right)A_3D_i^3\left(\frac{dw_s}{dt}\right)_i$$

$$=\sum_j F_{c,j\to i}^z+\frac{\rho}{2}C_DA_2D_i^2\sqrt{\left(u_f-u_{s,i}\right)^2+\left(w_f-w_{s,i}\right)^2}\left(w_f-w_{s,i}\right) \tag{20}$$

$$+\frac{\rho}{2}C_LA_2D_i^2\left|u_f-u_{s,i}\right|\frac{\partial\left(w_f-w_{s,i}\right)}{\partial z}-\rho\left(\frac{\rho_s}{\rho}-1\right)gA_3D_i^3$$

$$\frac{\pi D_i^3}{16}\left(\frac{d\omega_s}{dt}\right)_i=\sum_j F_{j\to i}^\eta \tag{21}$$

where ρ_s is the sediment density, A_2 and A_3 are the two and three-dimensional geometrical coefficient of sediment, respectively, $C_M = 0.5$ is the coefficient of added mass, $C_L = 4/3$ is the lift coefficient, C_D is the drag coefficient ($= 0.4 + 24/Re_s$), Re_s is the sediment Reynolds number ($= u_s D/\nu_0$), $u_{s,i}$ and $w_{s,i}$ denote the sediment particle velocity components in two dimensional coordinates.

The time integrations in the WCSPH and DEM models were implemented by semi-implicit and explicit algorithms, respectively. The characteristic time-step size of the DEM computations was much smaller than that of the WCSPH computations. To handle this problem, a multiple time-step algorithm was developed for the coupled model. Figure 3 describes the coupling algorithm of the WCSPH-DEM model.

3.4 Model Validation

The capability of the developed model in simulating standing wave hydrodynamics were discussed in depth in [Yeganeh-Bakhtiary et al., 2017] and the model was successfully validated against experimental measurements. To evaluate the effect of SPS turbulence model, the numerical results with and without the SPS model were compared Zhang et al. [2001] experimental data. Figure 4 shows the distribution of the non-dimensional horizontal component of wave orbital velocity (*UT*/*H*) against wave period at *z* =25 cm. *U*, *T* and *H* are the horizontal component of wave orbital velocity, wave period and wave height, respectively. Analysis of Figure 4 shows that, although the two cases of (with and without the SPS model) initially agree quite well with Zhang et al. [2001] data, the wave modeled without SPS model fitted much better with the experimental data and therefore the SPS turbulence closure model has robust performance.

Then the accuracy of the two-phase flow model developed in this study was verified by the transport rate under unidirectional flow condition. The bed flux under steady flow was simulated and the numerical results were compared to the experimental formula. The bed flux was chosen for two folds: (i) the steady streaming generated by standing wave is the key scouring mechanism, and (ii) the transport rate at sheet flow condition is predominant. The validation simulations were conducted with uniform spheres for the sediment phase, under the influence of different flow with varying Shields parameter (τ^*= 0.2, 0.4, 0.6 and 0.8). The physical characteristics of the test cases is summarized in Table 1. The Shields parameter τ^*, tested with the numerical simulations were equivalent to those reported in Hajivalie et al. [2012] experiments. The numerical results were compared to Meyer-Peter & Müller [1948] formulae (Eqs. 22 & 23).

$$q_b^* = \frac{q_b}{\sqrt{\left((\frac{\rho_s}{\rho} - 1)\right) g D^3}} = a(\tau^* - \tau_{cr}^*)^n \tag{22}$$

$$\tau^* = \frac{u_*^2}{\left((\frac{\rho_s}{\rho} - 1)\right) g D} \tag{23}$$

where q_b denotes bed flux, q_b^* is dimensionless bed flux, a and n are empirical constants, $\tau^*$and τ_{cr}^* are the Shields parameter and the critical Shields parameter, respectively. Based on the modified Shields diagram, the critical Shields parameter is set to $\tau_{cr}^* = 0.055$, and the values of $a = 8.5$, $n = 1.5$ were applied for the experimental formula. Given that in most of the scenarios modelled in this study, $\tau^* \geq 0.4$; therefore, the sheet flow is the predominate mode of transport [Fredsøe, 1993]. This study adopts Madsen & Grant [1976] suggestions and therefore used a modified constants of $a = 7.5$ and $n = 1.1$ to estimate the sheet flow mode of transport at higher values of shear stress ($\tau^* \geq 0.4$).

Figure 5 illustrates a schematic of the numerical domain for sediment transport simulation under steady unidirectional flow. Periodic boundary condition is applied for inlet and outlet particles of both fluid and sediment phases, in the direction of flow, to re-introduce the particles which pass through the outlet boundary of the computational domain [Zou, 2007]. In addition, two ghost domains with similar hydrodynamic characteristic to the main computational domain were employed to make up for the lack of influence domain for the lateral particles. Figure 6 confirms that good agreement exists between the numerical results and experimental formula (Eqs. 22 & 23) for bed-load sediment transport.

4. Scouring Simulation

The WCSPH-DEM two-phase flow model developed within this study (§3) is implemented for investigating scour – deposition processes in front of a vertical breakwater. The numerical results are compared to Xie [1981] laboratory investigations which were conducted in a 38 m long, 0.8 m wide and 0.6 m deep wave flume. Table 2 describes the numerical configurations based on physical characteristics of incident wave and sediment bed described in Xie [1981] laboratory investigations.

The sand grains simulated in this study are relatively fine and the sheet flow with suspension mode was observed in the numerical simulations. Sediment particle diameter was set to 4.0 mm in the DEM model for computational efficiency purposes, meaning each particle is the representative particle that represents the combination of few smaller particles. Using the representative particle approach for DEM is particularly well-justified for sheet flow mode of transport [Clayton et al., 2010]. Furthermore, for the large bed shear stress, sheet flow is the dominant mode of sediment transport for non-cohesive sediment grains [Fredsøe, 1993]. The

numerical simulations were conducted with using of Shields parameter based on the laboratory data.

Figure 7 displays the snapshots of the scour – deposition formation in front of a vertical breakwater for test No. 1. The figure shows the sediment particles are influenced by the top recirculating cells. Sand bars and scour holes started to form in the computational domain after few wave periods (~8T). The results show that sand particles deposited at antinodes in the vicinity of the vertical breakwater, at $L/2$ and L from the vertical breakwater. The scour hole formed between two consecutive sand bars at approximately $L/4$ and $3L/4$ from the vertical breakwater (at nodes). Figure 7 indicates the scour holes and sand bars progressively increased through the simulation and after approximately $48T$, the maximum scour depth is reached. A semi-equilibrium condition was reached after $60T$ and afterwards the bed sediment movement did not change the bed scour – deposition pattern.

Figure 8 compares the numerical results for the bed profile with that of Xie [1981] experiments for test Nos. 1- 4. It is evident that the numerical scour pattern fitted very well with the experimental result for the test Nos. 1-2, with $h/L = 0.150$. However, at the distance $L/2$ from the breakwater, the numerical model slightly over-predicted the experiments. The analysis of numerical results exhibits slight scatter between the numerical prediction and experimental measurements for the test cases with lower h/L values. The highest scatter between the experiments and numerical results was observed for the test case No. 4 with $h/L = 0.10$, where the maximum numerical scour at the distance of $L/2$ from the breakwater had 25% scatter from Xie [1981] measurements. The analysis of numerical results indicates that decreasing the h/L, increases the essential numerical time needed for reaching the equilibrium condition of scour –

deposition processes, meaning that for lower h/L the numerical model needs more simulation time to accurately approximate the maximum scouring depth.

The variation of non-dimensional scour depth (Z_{sm}/H) for the numerical model are determined at first node from the vertical breakwater and compared to Xie [1981] laboratory measurements (Figure 9). Term Z_{sm} denotes the maximum scour depth at the end of simulation time and H is the incident wave height. Figure 9 shows good agreement exists between the numerical results and experimental measurements, for the higher range of h/L. The WCSPH-DEM model developed within this study, is successfully estimated the bed profile and maximum scour depth; though a slight discrepancy between the numerical results and experimental measurements was observed, for the case with smaller h/L.

Figure 10 compares the non-dimensional time variation (t/T) versus scouring (Z_s/H) at first node from the vertical breakwater for test Nos. 1-4; Z_s represents the scour depth during the simulation time. The simulations show that reduction in h/L reduces the speed of scour-hole generation throughout the simulation. For the case of $h/L = 0.175$ the scour depth (Z_s/H) reached the equilibrium condition at $t/T = 50$, while for other test cases, more simulation time was required in order to reach the equilibrium state. The data trend in Figure 10 depicts Z_s/H follows a power law function ($x = t/T$ and $y = Z_s/H$), indicating that simulation time needs to be long enough to achieve the equilibrium condition for scour depth.

Figure 11 illustrates sediment transport modes at the vicinity of the first node from the vertical wall, where the horizontal orbital velocity is high. As seen, the sediment particles have different modes of transport based on their positions and accumulative condition. The analysis of numerical results shows that particles transport in four layers including, hyper-concentrated

layer, saltation layer, suspended particles and deposited layers. Sediment particles, in the hyper-concentrated layer, are primarily moving by impact of the contacting particles, resulting in relatively lower kinetic energy for the particles. Within the saltation layer, the saltating particles jump over the lower layer and the aggregation resulted from the moving sediment particles is low; however, particle's kinetic energy is higher compared to the hyper-concentrated layer. Thus, the motion of distinct particles is less influenced by the contact effects in the saltation layer. In the suspended layer, particle aggregation is the least and sediment particles are moving with the highest kinetic energy, with an occasional collision of particles. The energetic behavior of sediment in suspended layer occur due to the strong interaction between sediment particles and the top recirculating fluid cells.

The analysis of numerical results indicates that movement of sediment particles in the deposited layer are different compared to the other three layers. Figure 12 displays the sediment particle movements within the deposited layer, in the vicinity of the first node from the vertical wall. Blue arrows in the figure show the direction of sediment motion and black lines indicate the path of sediment particles. Partial recirculating modes in the sediment phase, similar to the steady streaming recirculating cells in the fluid phase, was observed, for the first time, from the numerical simulations (Figure 12). The exchange and transfer of momentum between the upper layer of sediments and fluid particles, phase-lag in sediment layers and fluid particle movements, interparticle collisions as well as the existence of shear stress between the particles are responsible for the recirculating mode observed in the sediment phase. The occurrence of recirculating cells in the sediment layer has not been reported in the previous studies.

Fluid-sediment interactions during the scour – deposition process are further studied by comparing the horizontal velocity of sediment particles and horizontal orbital velocity of fluid particles during a wave period at the halfway between first node and antinode from the vertical wall. Figure 13 presents the horizontal velocity variation against the non-dimensional sediment particle layers, y/d_p, where d_p is the sediment particle diameter. The height range, between $7d_p$ to $11d_p$, relates to the hyper-concentrated layer; $11d_p$ to $13d_p$ is within the saltation layer, and values higher than $13d_p$ depicts the suspended particle layer. Further analysis of numerical results show that after a short time from the start of the simulation ($t \approx T/6$), the sediment particles accelerated their motion and reached to similar horizontal velocity as the fluid particles. At $t = 3T/6$ the horizontal velocity of sediment particles exceeded the fluid particles, and after $4T/6$ a time-lag difference was clearly noticed. Figure 13 illustrates that in the upper part of the water column when the direction of fluid flow changes, the sediment particle acceleration increases due to bore and undertow motion. Hence, the interphase momentum is transferred remarkably from the fluid phase to the sediment phase at $\approx T/2$.

The snapshots of horizontal velocity of sediment particles in the deposited layer and over a wave period are shown in Figure 14. It is evident that the sediment particles started their motion with lower velocity compared to the fluid particles in the upper layers of the computational domain. This layer of sediment was not influenced by fluid flow directly; however, the vertical momentum transfers from particle motions in the upper layers affected the movement of deposited layer.

Figure 15 investigates the relation between the scour – deposition pattern and the steady streaming velocity near the bed, by comparing the scour – deposition patterns for all the test

cases within $L/2$ distance in front of the vertical wall. The figure shows that for $h/L = 0.15$ the highest steady streaming velocity (red line in the figure) and sediment deposition rate near the wall is occurred. In contrast, the simulation results for the case of $h/L = 0.175$ is completely inverse with regards to the deposition rate and scour hole lengthening. For the test cases with $h/L = 0.10$ and $h/L = 0.125$, the steady streaming velocity and scour – deposition patterns are nearly the same. Therefore, it could be concluded from Figure 15, that increasing the steady streaming velocity near the bed, results in an increase in the deposition rate and the depth of scour hole.

Figure 16 illustrates the ratio of the suspended load to the total load of sediment transport and the horizontal orbital velocity during a full wave cycle at the distance of $L/8$ from the vertical wall. The figure shows, for $h/L = 0.15$ and $h/L = 0.175$, the highest and the lowest percentage of suspended sediment load was observed, respectively, while for the test cases with $h/L = 0.10$ and $h/L = 0.125$, the amount of suspended sediment load was nearly equal.

5. Conclusions

A Lagrangian two-phase model is developed for simulating the scouring processes in front of vertical breakwaters. The fluid phase is simulated using the solution of 2D Navier-Stokes equations in the weakly compressible smoothed particle hydrodynamics (WCSPH) formation in conjunction with the SPS turbulence closure model (§3.1). The sediment phase is simulated using MBS method and through computing the effects of interparticle and particle-wall collisions by activating a spring-dashpot system (§3.2). Comparison between the numerical simulations and experimental measurement of Xie [1981] confirmed that the two-phase WCSPH-DEM

model described in this paper is robust and capable of successful estimation of bed form and the maximum scour depth when a semi-equilibrium condition was reached.

The analysis of the simulation results shows the controlling sediment transport mode was sheet flow with suspension, which confirms the reliability of the model in simulation of scour – deposition processes. It was also found that the ratio of h/L impacts the computational time needed to reach the semi-equilibrium condition, smaller h/L resulted in higher simulation time in order to reach the semi-equilibrium condition.

Further analysis of the numerical results revealed that partial recirculating pattern of sediment particles movement, similar to the steady streaming recirculating cells in the fluid phase, exists in the deposited layer. The recirculating pattern of sediment particles is caused by the transfer of momentum from upper layer of sediment particles, phase-lag between sediment layers and fluid phase movements, interparticle collisions, and the existence of shear stress between particles. The sediment particles in the deposited layer were mainly influenced by the vertical momentum transferring from the upper layers and moved with very low velocity.

Time-lag between flow and sediment velocity was observed, which is mainly due to the sediment inertia and transferring rate of momentum. The results indicated that the interphase momentum was transferred significantly from the fluid phase to the sediment phase at nearly $t = T/2$.

Furthermore, it is apparently found that increasing the steady streaming velocity near the bed, accelerates the deposition rate and increases the depth of scour hole. A direct link between the deposition rate and growth in the suspended-load ratio, was observed. For all the test cases,

suspended sediment load reached the maximum level at $t = T/4$ during the shoreward bore action and $t = 3T/4$ during the seaward undertow action. The numerical results confirm that the proposed model in this study is robust and effective tool to simulate the scouring process in front of the vertical coastal defenses.

6. Acknowledgment

The authors would like to thank Dr. Fatemeh Hajvalie for her constructive comments on the development of numerical model.

7. References

Abolfathi, S., Shudi, D., Borzooei, S., Yeganeh-Bakhtiari, A. & Pearson, J. [2018] "Application of Smoothed Particle Hydrodynamics in evaluating the performance of coastal retrofit structures," Proc. 34th International Conference of Coastal Engineering (ICCE). [S.l.], Paper 109. ISSN 2156-1028. doi:https://doi.org/10.9753/icce.v36.

Ataie-Ashtiani, B. & Mansour-Rezaei. S. [2009] "Modification of Weakly Compressible Smoothed Particle Hydrodynamics for Preservation of Angular Momentum in Simulation of Impulsive Wave Problems," Coastal Engineering Journal. **51** (4), 363-386.

Blinn, L., Hadjadj, A. & Vervisch, L. [2002] "Large eddy simulation of turbulent flows in reversing systems," Proc. 1st French Seminar on Turbulence and Space Launchers. CNES, Paris, 2002.

Chen, B. [2007] "The numerical simulation of local scour in front of a vertical-wall breakwater," Journal of Hydrodynamics, Ser. B. **18** (3), 134-138.

Clayton T. C., Schwarzkopf J. D., Sommerfeld M. & Tsuji Y. [2011] "Multiphase Flows with Droplets and Particles" 2nd Edition, CRC Press, p. 509.

Crespo, A. J. C., Gómez-Gesteira, M. & Dalrymple, R. A. [2007] "Boundary conditions generated by dynamic particles in SPH methods," Computers, Materials and Continua. **5**(3), 173-184.

Cundall, P. A. & Strack, O. D. [1979] "A discrete numerical model for granular assemblies," Géotechnique. **29** (1), 47–65.

Dalrymple, R. A. & Rogers, B. D. [2006] "Numerical modelling of water waves with the SPH method," Coastal Engineering. **53**(2-3), 141-147.

de Best, A. & Bijker, E. W. [1971] "Scouring of a sand bed in front of a vertical breakwater", Communications on Hydraulics, Report No. 71-1, Department of Civil Engineering, Delft University of Technology.

Dong, S., Salauddin, M., Abolfathi, S., Tan, Z. H. & Pearson, J. M. [2018] "The Influence of Geometrical Shape Changes on Wave Overtopping: A Laboratory and SPH Numerical Study," Coasts, Marine Structures and Breakwaters 2017. 1217-1226.

Fernandez, J. W., Cleary, P. W., Sinnott, M. D. & Morrison, R. D. [2011] "Using SPH one-way coupled to DEM to model wet industrial banana screens," Minerals Engineering. **24**, 741–753.

Fredsøe, J. [1993] "Modelling of non-cohesive sediment transport processes in the marine environment" Coastal Engineering. **21**(1–3), 71-103.

Gíslason, K., Fredsøe, J., Deigaard, R. & Sumer, M. [2009a] "Flow under standing waves; Part 1. Shear stress distribution, energy flux and steady streaming," Coastal Engineering. **56** (3), 341–362.

Gislason, K., Fredsoe, J. & Sumer, B. M. [2009b] "Flow under standing waves; part 2- scour and deposition in front of breakwaters," Coastal Engineering. **56** (3), 363–70.

Gotoh, H. & Kahyyer, A. [2018] "On the state-of-the-art of particle methods for coastal and ocean engineering," Coastal Engineering Journal. **60** (1), 79-103.

Gotoh, H. & Sakai, T. [1999] "Lagrangian Simulation of Breaking Waves Using Particle Method," Coastal Engineering Journal. **41** (3-4), 303-326.

Gotoh, H., Ikari, H., Memita. T. & Sakai, T. [2005] "Lagrangian Particle Method for Simulation of Wave Overtopping on a Vertical Seawall," Coastal Engineering Journal. **47** (2-3), 157-181.

Gotoh, H., Shao, S. & Memita, T. [2004] "SPH-LES Model for Numerical Investigation of Wave Interaction with Partially Immersed Breakwater," Coastal Engineering Journal. **46** (1), 39-63.

Gotoh, H., Shibahara, T. & Sakai, T. [2001] "Sub-particle-scale turbulence model for the MPS method Lagrangian flow model for hydraulic engineering," Comput. Fluid Dyn. J. **9** (4), 339-347.

Hajivalie, F., Yeganeh-Bakhtiary, A., Houshangi, H. & Goto, H. [2012] "Euler–Lagrange model for scour in front of vertical breakwater," Applied Ocean Research. **34**, 96–106.

Harada, E., Gotoh, H., Ikari, H. & Khayyer, A. [2019] "Numerical simulation for sediment transport using MPS-DEM coupling model," Advances in Water Resources. **129**, 354-364.

Harada, E., Ikari, H., Shimizu, Y., Gotoh, H. & Khayyer, A. [2018] "Numerical investigation of the morphological dynamics of a step-and-pool riverbed using DEM-MPS," Hydraulic Engineering. **144** (1), 04017058.

He,Y. Bayly, A. E., Hassan, A. Yang, D. & Muller, F., K. [2018] "A GPU-based coupled SPH-DEM method for particle-fluid flow with free surfaces," Powder Technology. **338**, 548-562.

Huang, Y. J. & Nydal, O. J. [2012] "Coupling of discrete-element method and smoothed particle hydrodynamics for liquid-solid flows," Theor. Appl. Mech. Lett. **2**(1), doi.org/10.1063/2.1201202.

Hughes, S. A. & Fowler, J. E. [1991] "Wave-induced scour prediction at vertical walls," Proc. conference coastal sediments. **91**, 1886-1899.

Irie, I. & Nadaoka, K. [1984] "Laboratory reproduction of seabed scour in front of breakwaters," Proc. 19th International Conference on Coastal Engineering (ICCE). Houston, TX. 2 (26), 1715- 1731.

Khayyer, A. & Gotoh, H. [2008] "Development of CMPS Method for Accurate Water-Surface Tracking in Breaking Waves," Coastal Engineering Journal. **50** (2), 179-207.

Khayyer, A., Gotoh, H. & Shao, S. D. [2008] "Corrected incompressible SPH method for accurate water-surface tracking in breaking waves," Coastal Engineering. **55**, 236-250.

Khayyer, A., Gotoh, H., Shimizu, K., Gotoh, K., Falahaty, H. & Shao, S. D. [2018] "Development of a projection-based SPH method for numerical wave flume with porous media of variable porosity," Coastal Engineering. **140**, 1-22.

Lillycrop, W. J. & Hughes, S. A. [1993] "Scour hole problems experienced by the Corps of Engineers; Data presentation and summary," Miscellaneous papers. CERC-93-2, US Army Engineer Waterways Experiment Station. Coastal Engineering Research Center, Vicksburg, MS.

Madsen, O. S. & Grant, W. D. [1976] "Quantitative description of sediment transport by waves," In: Proceedings of the 15th Int'l Conference Coastal Engineering: ASCE. 1093–1112.

Meyer-Peter, E. & Müller, R. [1948] "Formulas for bed-load transport," Proc. 2nd IAHR Congress. 39–64.

Monaghan, J. J. & Kocharyan, A. [1995] "SPH simulation of multi-phase flow," Computer Physics Communications. **87**, 225–235.

Monaghan, J. J. & Lattanzio, J. C. [1985] "A refined particle method for astrophysical problems," Astron. Astrophys. **149**, 135–143.

Monaghan, J.J. [1992] "Smoothed particle hydrodynamics" Annu. Rev. Astron Astrophys. **30**, 543–74.

Monaghan, J. J. [1994] "Simulating free surface flows with SPH," Computational Physics. **110**, 399 - 406.

Monaghan, J. J. [2005] "Smoothed particle hydrodynamics," Rep. Prog. Phys. **68**, 1703–1759.

Morris, J. P., Fox, P. J. & Zhu, Y. [1997] "Modeling low Reynolds number incompressible flows using SPH," Computational Physics. **136**, 214–226.

Oumeraci, H. [1994a] "Review and analysis of vertical breakwater failures — lessons learned," Coastal Engineering, Special Issue on Vertical Breakwaters. **22**, 3–29.

Oumeraci, H. [1994b] "Scour in front of vertical breakwaters - review of problems," Proc. International Workshop on Wave Barriers in Deep Water. Port and Harbour Research Institute, Yokosuka, Japan, 281–307.

Potapov, A. V., Hunt, M. L. & Campbell, C. S. [2001] "Liquid–solid flows using smoothed particle hydrodynamics and the discrete element method," Powder Technology. **116**, 204–213.

Shao, S. D. & Lo, E. Y. M. [2003] "Incompressible SPH Method for Simulating Newtonian and Non-Newtonian Flows with a Free Surface," Advances in Water Recourses. **26** (7), 787-800.

Shao, S. & Gotoh., H. [2004] "Simulating Coupled Motion of Progressive Wave and Floating Curtain Wall by SPH-LES Model," Coastal Engineering Journal. **46** (2), 171-202.

Shao, S., Ji, C., Graham, D. I., Reeve, D. E, James, P. W. & Chadwick, A. J. [2006] "Simulation of wave overtopping by an incompressible SPH model," Coastal Engineering. **53**, 723-735.

Smagorinsky, J. [1963] "General circulation experiments with the primitive equations I. The basic Experiment," Monthly Weather Rev. **91**, 99–164.

Sumer, B. M. & Fredsøe, J. [2002] "The Mechanics of Scour in the Marine Environment," World Scientific, Singapore, xiv + 536 p.

Sumer, B.M. & Fredsøe, J. [2000] "Experimental study of 2D scour and its protection at a rubble-mound breakwater," Coastal Engineering. **40**, 59–87.

Tahersima, M., Yeganeh-Bakhtiary, A. & Hajivalie, F. [2011] "Scour pattern in front of vertical breakwater with overtopping," Coastal Research. **64**, 598-602.

Tofany, N., Ahmad M. F., Kartono, A., Mamat M. & Husain, M. L. [2014] "Numerical modeling of the hydrodynamics of standing wave and scouring in front of impermeable breakwaters with different steepnesses," Ocean Engineering. **88**, 255-270.

Tsuruta, N., Gotoh, H., Suzuki, K., Ikari, H. & Shimosako, K. [2019] "Development of PARISPHERE as the particle-based numerical wave flume for coastal engineering problems," Coastal Engineering Journal. **61** (1), 79-103.

Wang, D., Li, S., Arikawa., T. & Gen, H. [2016] "ISPH Simulation of Scour Behind Seawall Due to Continuous Tsunami Overflow," Coastal Engineering Journal. **58** (3), doi.org/10.1142/S0578563416500145.

Wang L, Khayyer A, Gotoh H, Qin Jiang, Q. & Zhanga, C. [2019] "Enhancement of pressure calculation in projection-based particle methods by incorporation of background mesh scheme," Applied Ocean Research. **86**, 320-339.

Xie, S. L. [1981] "Scouring pattern in front of vertical breakwaters and their influence on the stability of the foundation of the breakwaters," Report, Department of Civil Engineering, Delft University of technology, Delft, Netherlands, 61 p.

Yeganeh, A. Y., Gotoh, H. & Sakai, T. [2000] "Applicability of Euler–Lagrange coupling multiphase-Flow model to bed-load transport under high bottom shear," Hydraulic Research. **38** (5), 389–98.

Yeganeh-Bakhtiary, A., Hajivalie, F. & Hashemi-Javan, A. [2010] "Steady streaming and flow turbulence in front of vertical breakwater with wave overtopping," Applied Ocean Research. **32** (1), 91–102.

Yeganeh-Bakhtiary, A., Houshangi, H., Hajivalie, F. & Abolfathi, S. [2017] "A Numerical Study on Hydrodynamics of Standing Waves in front of Caisson Breakwaters with WCSPH Model," Coastal Engineering Journal. **59** (2), doi.org/10.1142/S057856341750005X.

Yeganeh-Bakhtiary, A., Shabani, B., Gotoh, H. & Wang, S. S. Y. [2009] "A three-dimensional distinct element model for bed-load transport," Hydraulic Research. **47** (2), 203–12.

Zanganeh, M., Yeganeh-Bakhtiary, A. & Abd Wahab, A. K. [2012] "Lagrangian coupling two-phase flow model to simulate current-induced scour beneath marine pipelines," Applied Ocean Research. **38**, 64–73.

Zhang, S., Kuwabara, S., Suzuki, T., Kawano, Y., Morita, K. & Fukuda, K. [2009] "Simulation of solid–fluid mixture flow using moving particle methods," Computational Physics. **228**, 2552–2565.

Zheng, X., Shao, S., Khayyer, A., Duan, W., Ma, Q. & Liao, K. [2017] "Corrected First-Order Derivative ISPH in Water Wave Simulations," Coastal Engineering Journal. **59** (1), doi.org/10.1142/S0578563417500103

Zou, S. [2007] "Coastal sediment transport simulation by Smoothed Particle Hydrodynamics," PhD Dissertation. The Johns Hopkins University.

Captions:

Table Captions:

Table 1: The physical characteristic of the sediment transport under unidirectional flows

Table 2: Test cases of numerical simulation based on Xie [1981] experiment

Figure Captions:

Figure 1: Schematic pattern of scour – deposition for a) coarse sand and b) fine sand.

Figure 2: Interaction between fluid and sediment particles in two-phase flow model

Figure 3: SPH-DEM coupling algorithm

Figure 4: Comparison of non-dimensional horizontal component of the wave orbital velocity between experimental values and numerical results with/without SPS model at z =25 cm

Figure 5: The numerical Computational domain for simulation of the sediment transport under unidirectional flow.

Figure 6: The dimensionless bed flux against Shields stress.

Figure 7: Pattern of scour – deposition in front of vertical breakwater for test No. 1

Figure 8: Comparison of scour profiles between numerical and experiment for test Nos. 1-4

Figure 9: Comparison of maximum scour depth between numerical and experimental values

Figure 10: Developing scour depth at 1st node in front of vertical breakwaters

Figure 11: Sediment transport modes at L/4 from the vertical breakwater for test No. 1

Figure 12: Formation of sediment transport recirculating cells during scour development in the deposited layer at L/4 from the vertical breakwater for test No. 1

Figure 13: Horizontal velocity for fluid and sediment during a wave cycle for test No. 1

Figure 14: Horizontal velocity of sediment particles in the domain of zero fluid velocity within a full wave cycle for test No. 1

Figure 15: Steady streaming velocity and scour profile within L/2 near the vertical breakwaters for Test. No 1 to 4, steady streaming velocity (top), bed profile (bottom)

Figure 16: Horizontal orbital velocity and suspended load ratio during a wave period, horizontal orbital velocity (top), suspended load ratio (bottom)

Table 1: The physical characteristic of the sediment transport under unidirectional flows

No	$D\ (mm)$	$\rho_s\ (\frac{kg}{m^3})$	$u\ (m/s)$	τ^*	u_*
1	4	2650	0.3	0.2	0.0197
2	4	2650	0.3	0.4	0.0278
3	4	2650	0.3	0.6	0.0341
4	4	2650	0.3	0.8	0.0394

Table 2: Test cases of numerical simulation based on Xie [1981] experiment

Test No.	T (s)	L (m)	H (m)	h (m)	$\frac{h}{L}$	$\frac{H}{L}$	D_{50} (mm)	ρ_s $(\frac{kg}{m^3})$	Sand Type	$Z_{s,m}$ (cm)	Simulation Time (s)
1	1.17	1.714	0.05	0.30	0.175	0.0292	4.0	2650	Fine	1.3	60T
2	1.32	2.00	0.075	0.30	0.15	0.0375	4.0	2650	Fine	2.8	60T
3	1.53	2.40	0.055	0.30	0.125	0.0229	4.0	2650	Fine	2.8	60T
4	1.86	3.00	0.055	0.30	0.10	0.0183	4.0	2650	Fine	4.0	60T

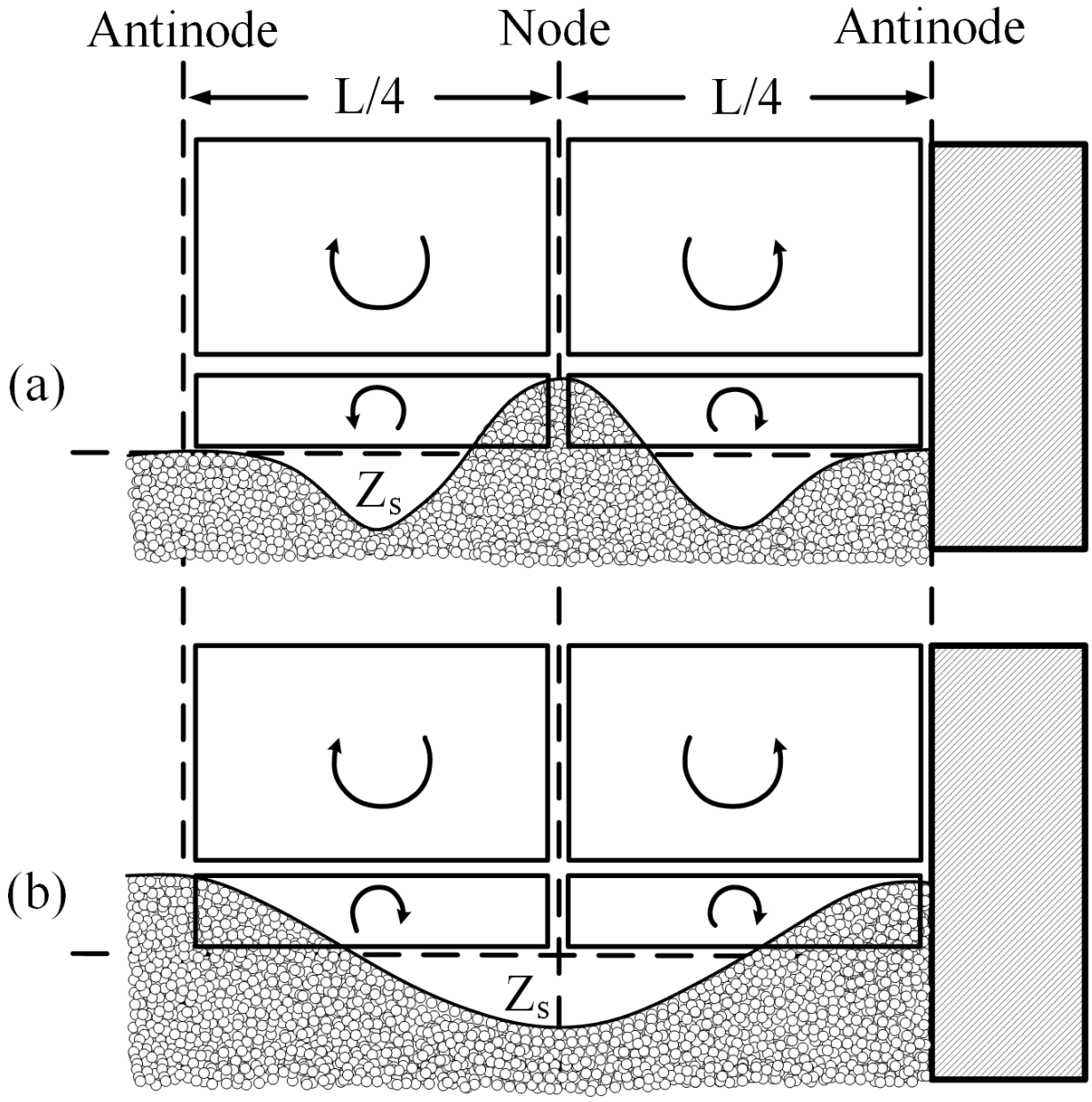

Figure 2: Schematic pattern of scour – deposition for a) coarse sand and b) fine sand.

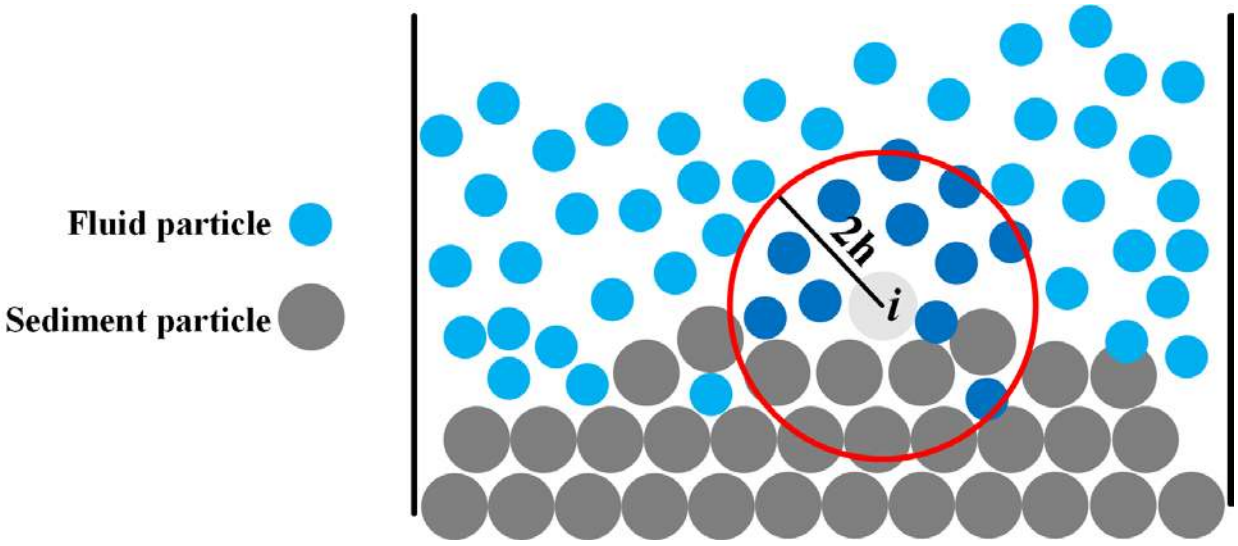

Figure 2: Interaction between fluid and sediment particles in two-phase flow model

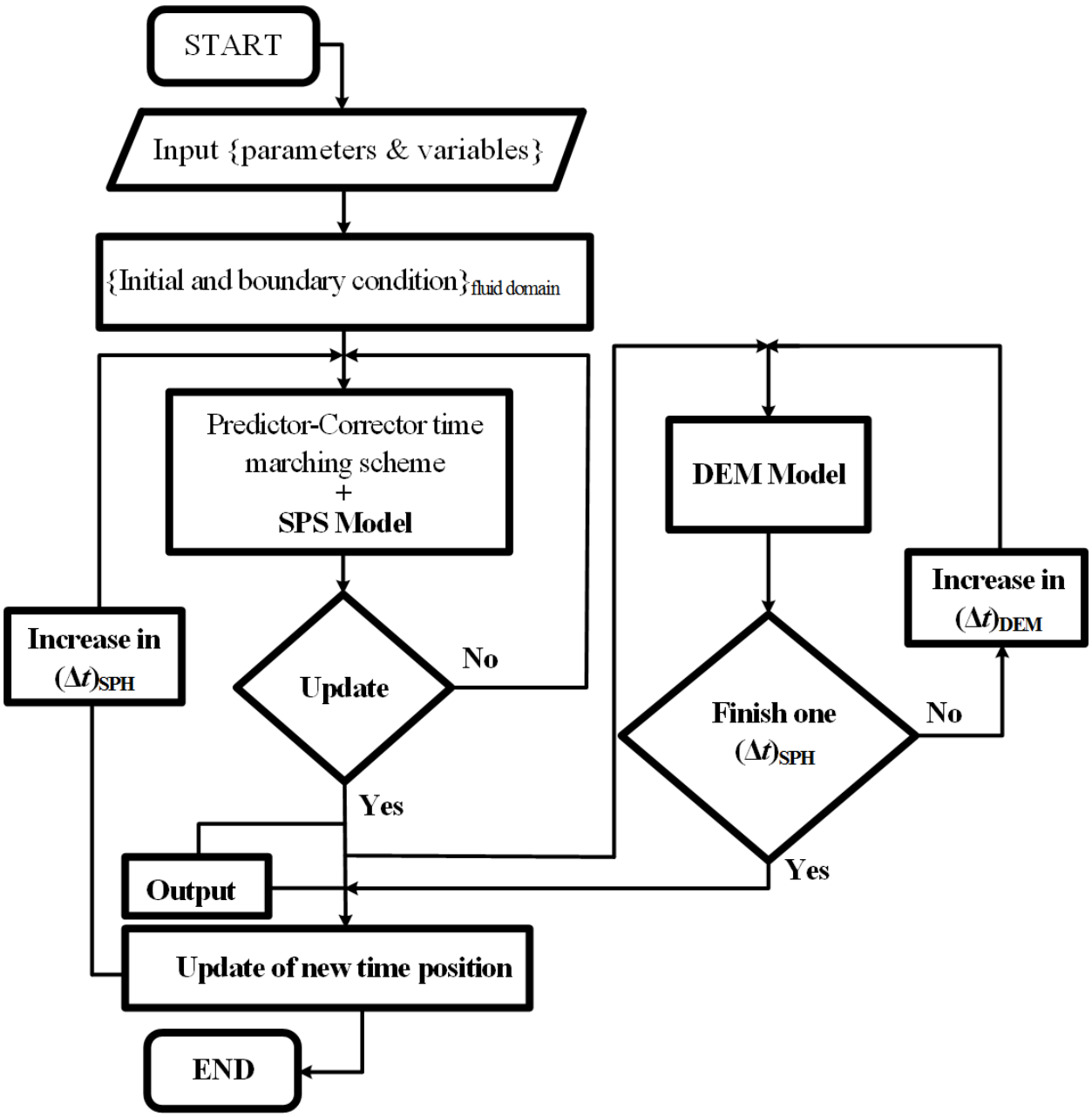

Figure 3: SPH-DEM coupling algorithm

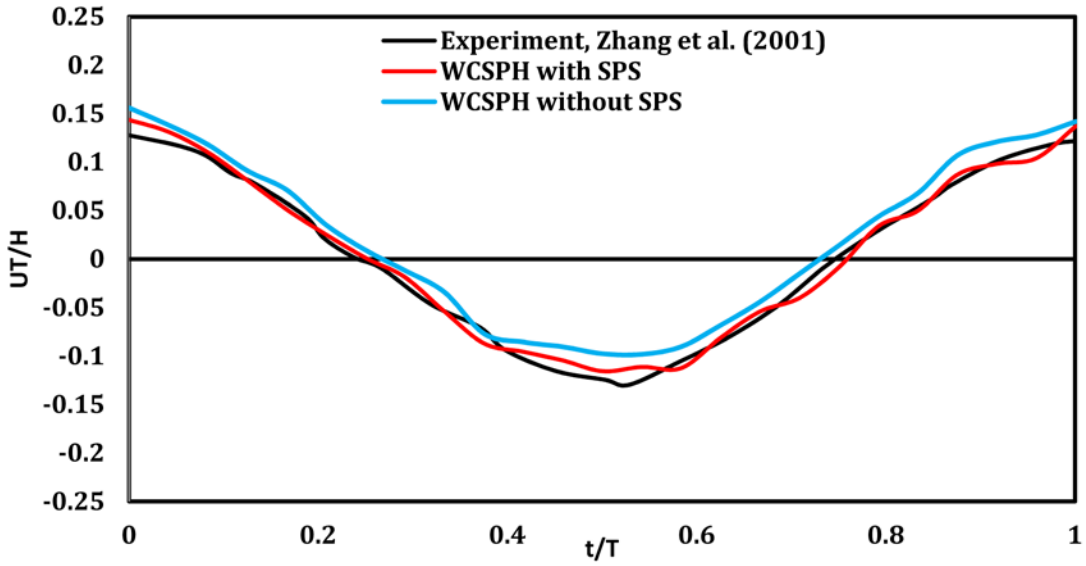

Figure 4: Comparison of non-dimensional horizontal component of the wave orbital velocity between experimental values and numerical results with/without SPS model at z =25 cm

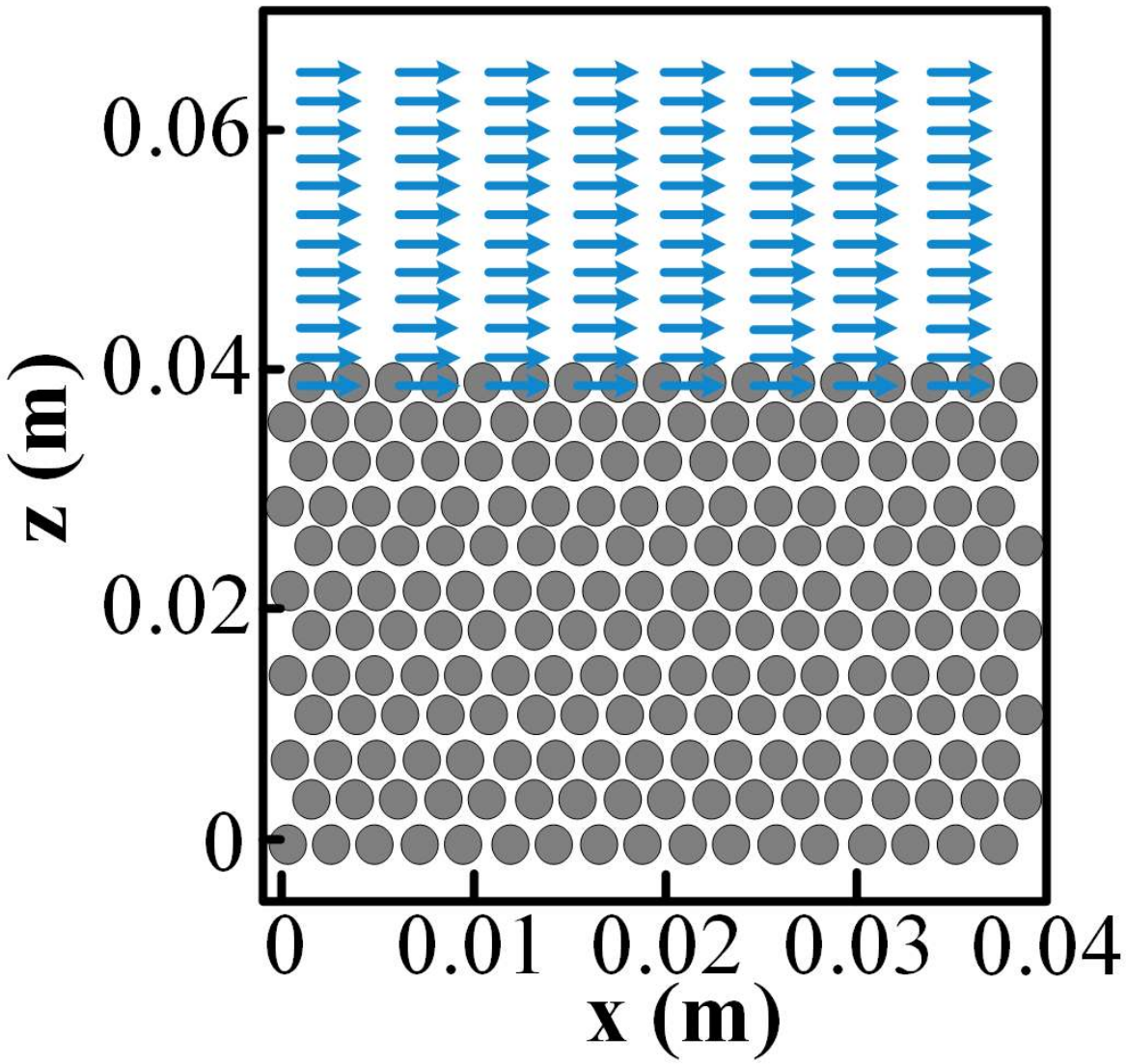

Figure 5: The numerical Computational domain for simulation of the sediment transport under unidirectional flow.

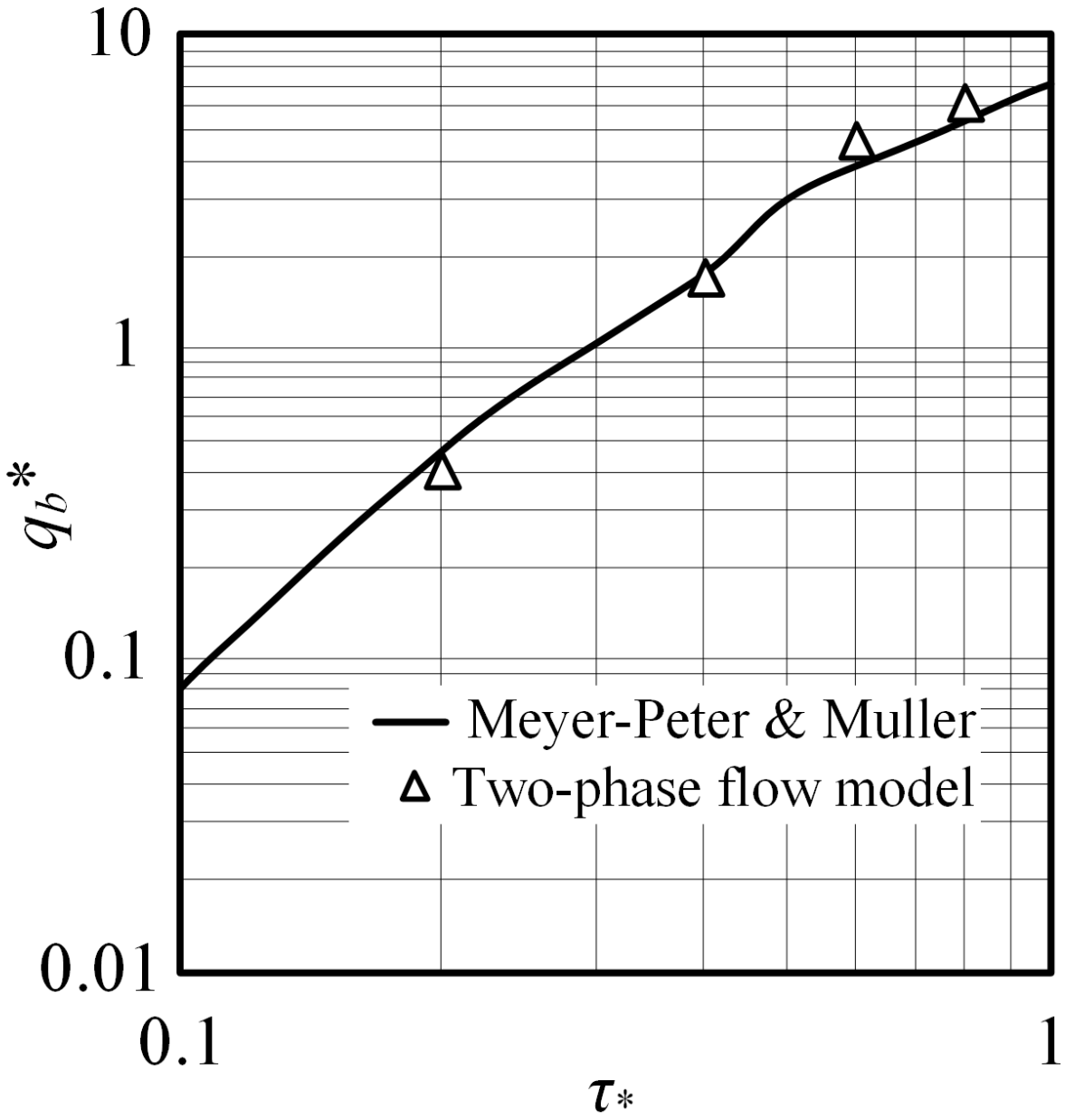

Figure 6: The dimensionless bed flux against Shields stress.

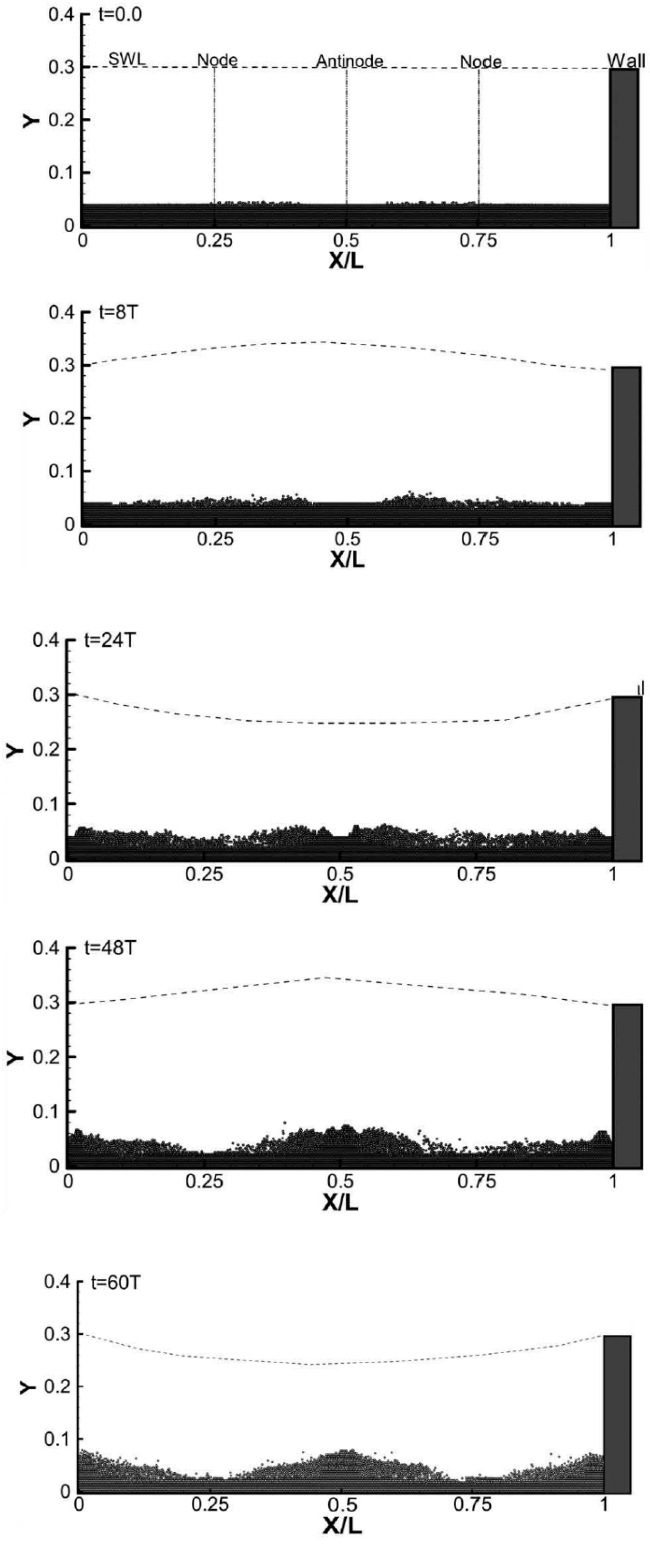

Figure 7: Pattern of scour – deposition in front of vertical breakwater for test No. 1

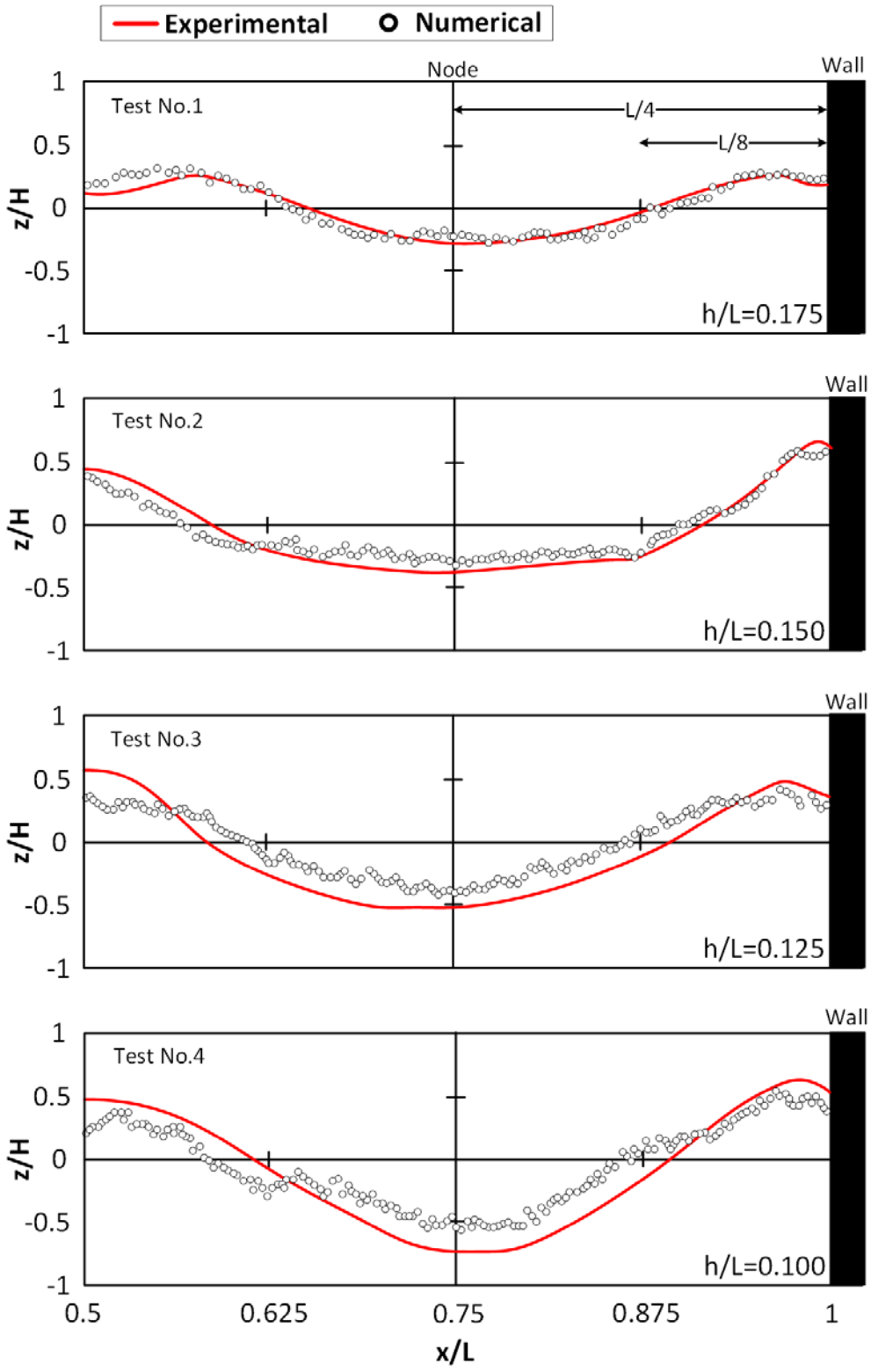

Figure 8: Comparison of scour profiles between numerical and experiment for test Nos. 1-4

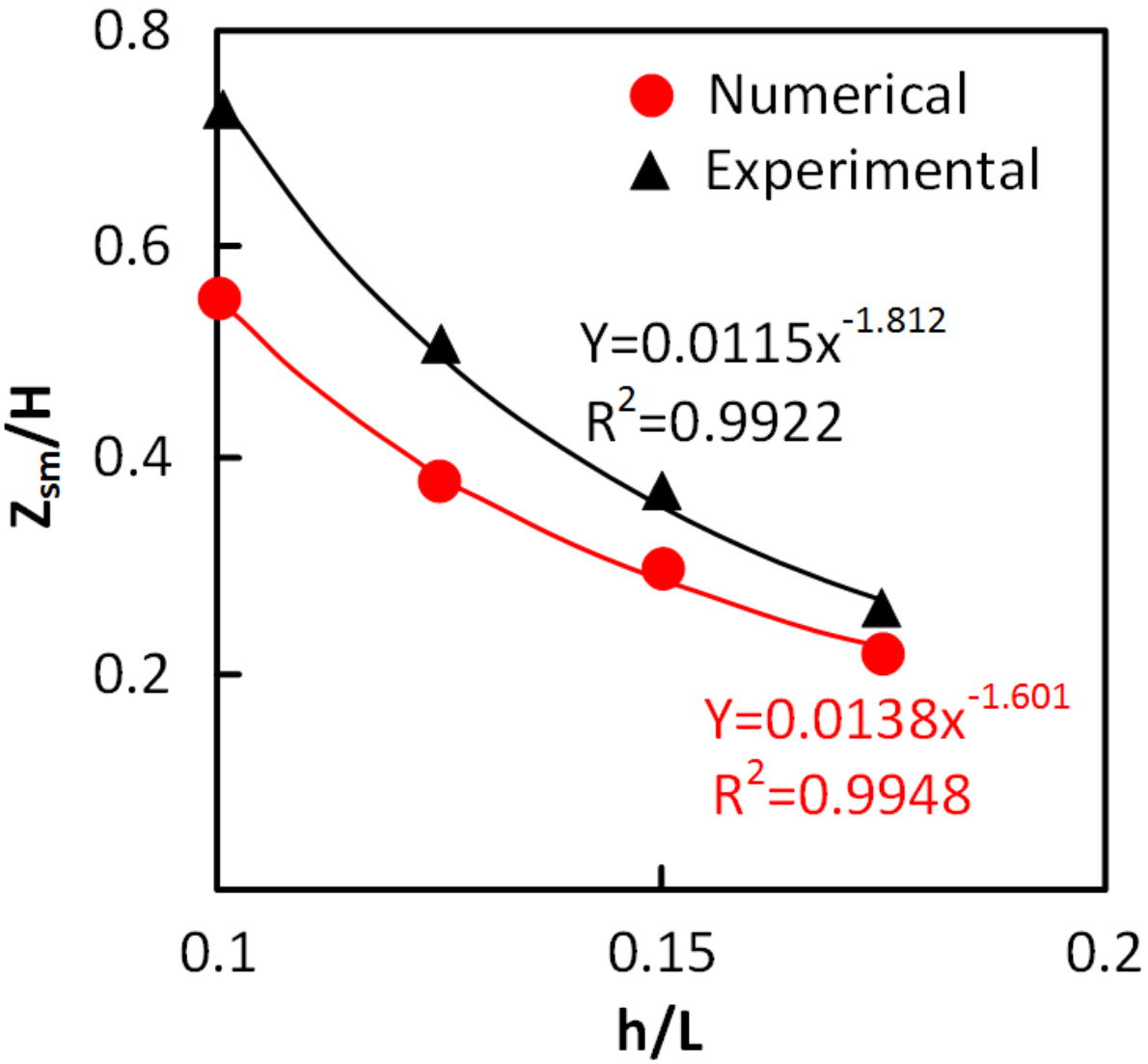

Figure 9: Comparison of maximum scour depth between numerical and experimental values

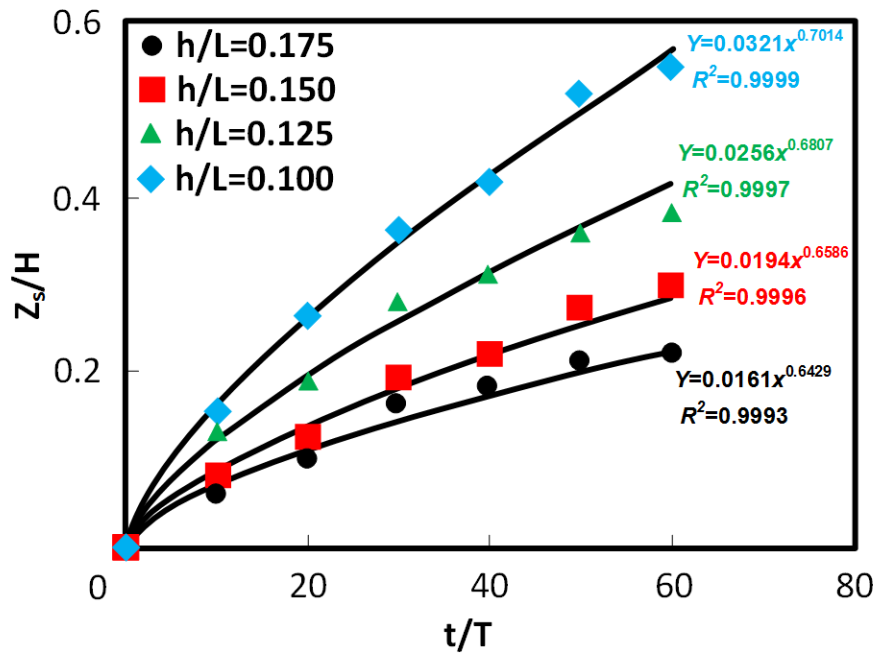

Figure 10: Developing scour depth at 1st node in front of vertical breakwaters

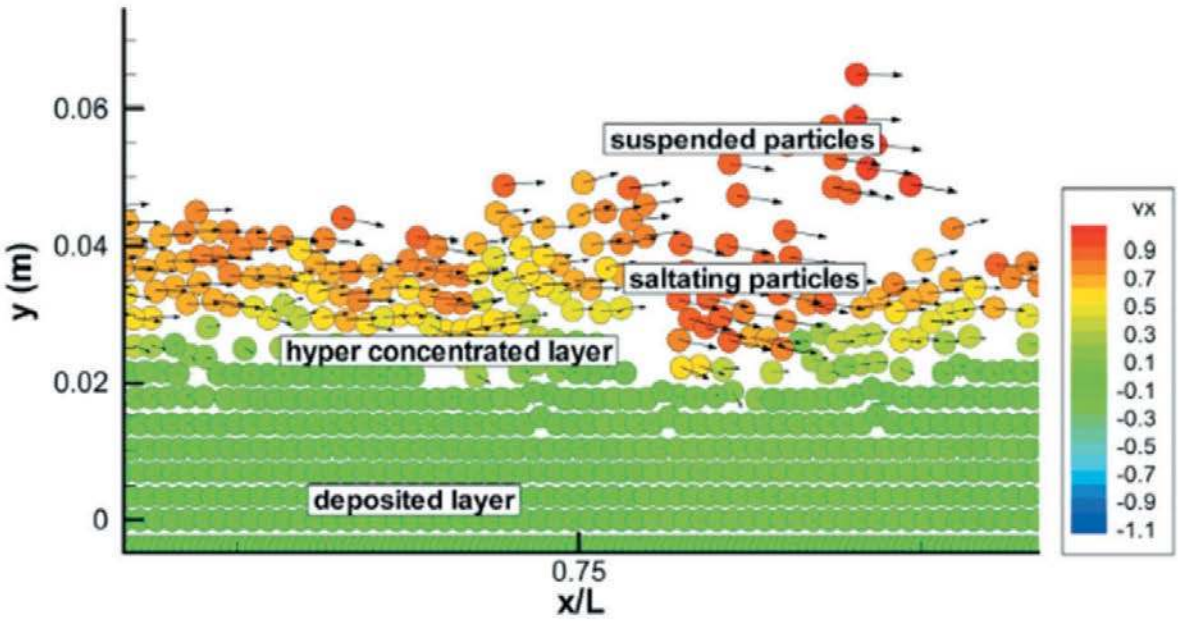

Figure 11: Sediment transport modes at L/4 from the vertical breakwater for test No. 1

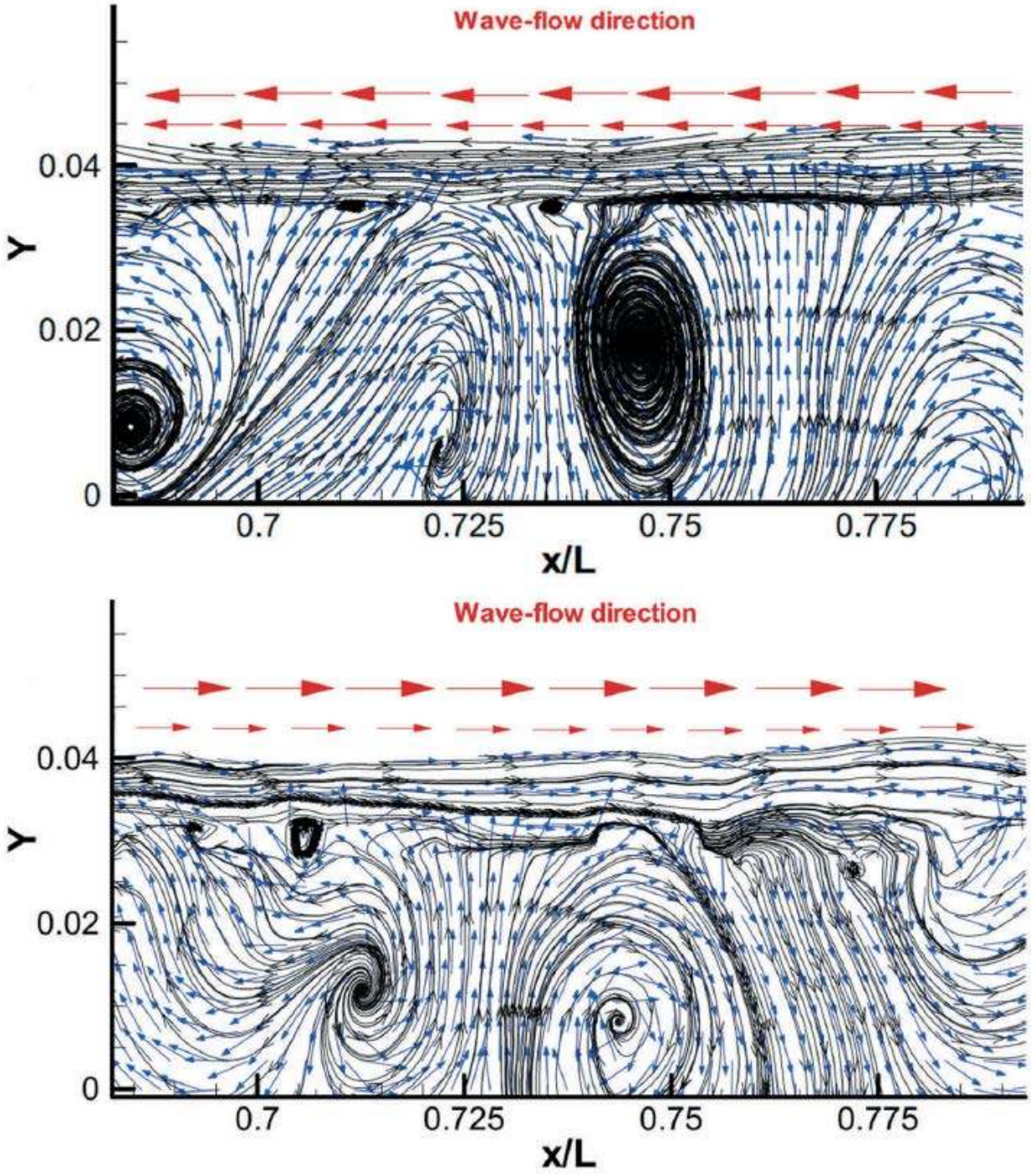

Figure 12: Formation of sediment transport recirculating cells during scour development in the deposited layer at L/4 from the vertical breakwater for test No. 1

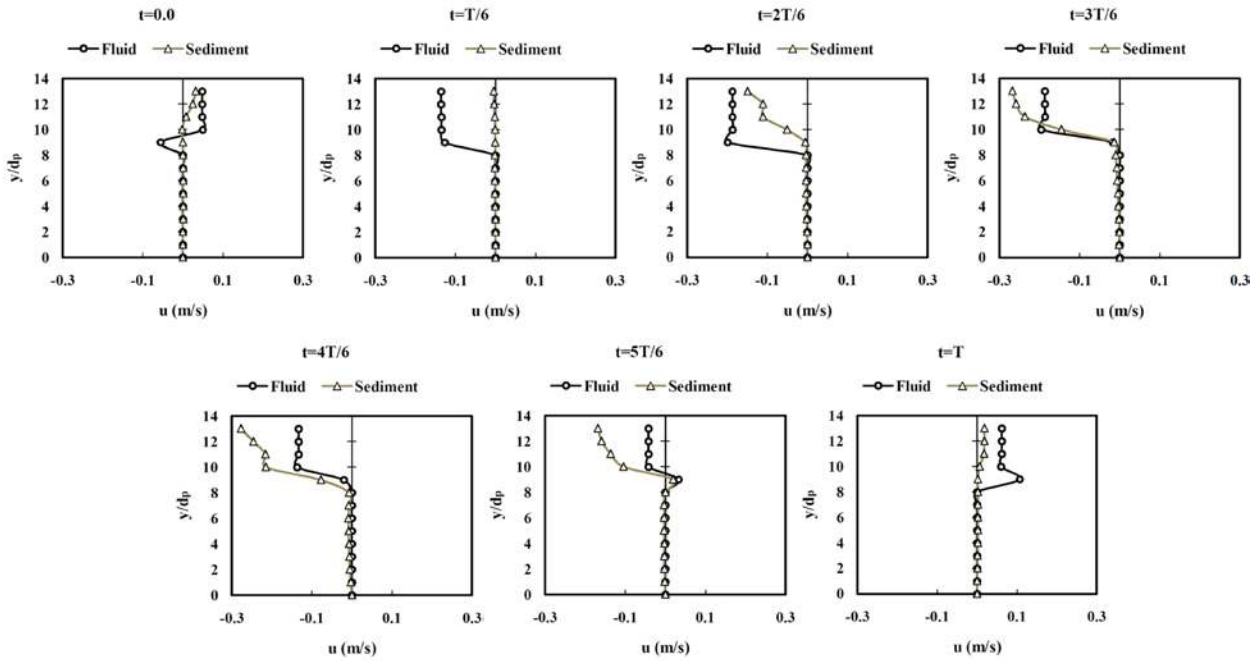

Figure 13: Horizontal velocity for fluid and sediment during a wave cycle for test No. 1

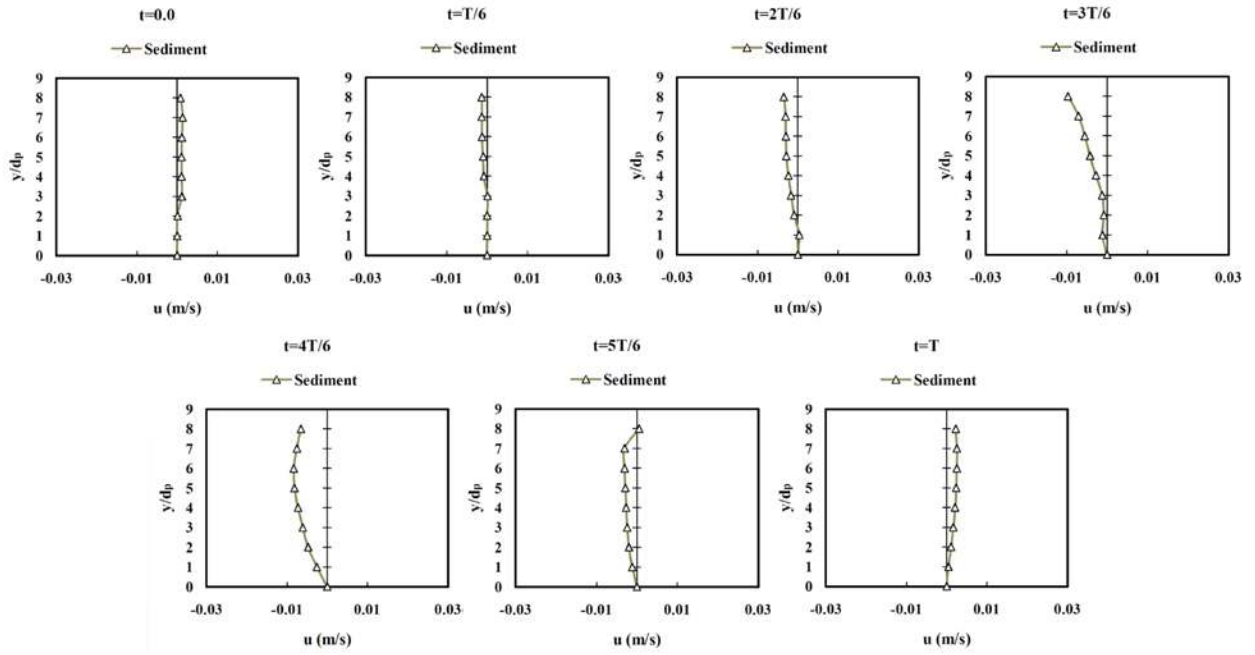

Figure 14: Horizontal velocity of sediment particles in the domain of zero fluid velocity within a full wave cycle for test No. 1

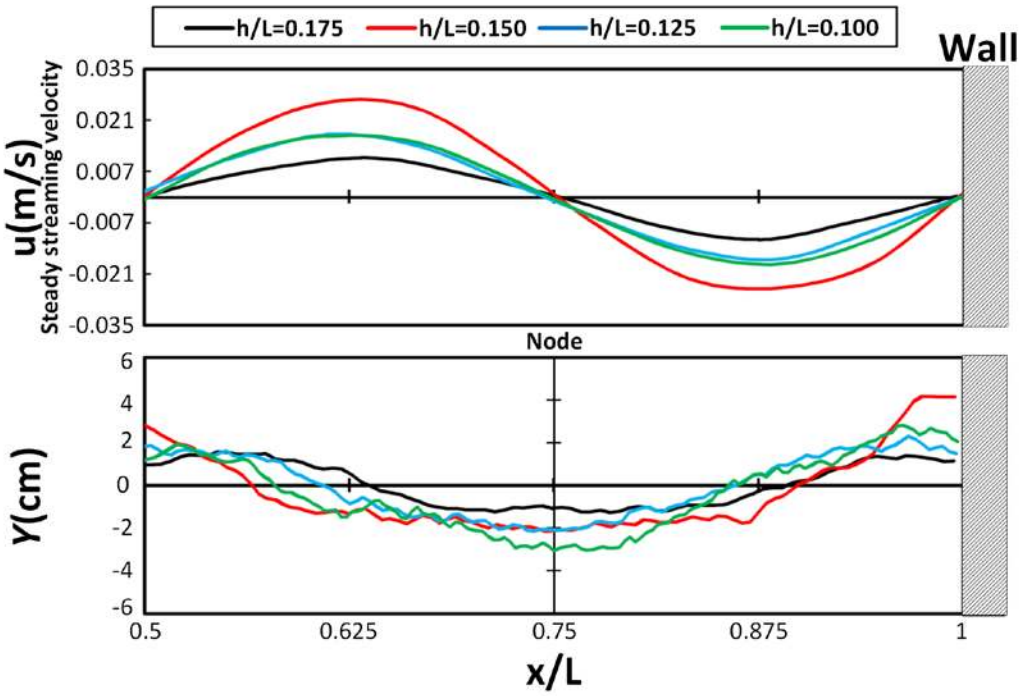

Figure 15: Steady streaming velocity and scour profile within L/2 near the vertical breakwaters for Test. No 1 to 4, steady streaming velocity (top), bed profile (bottom)

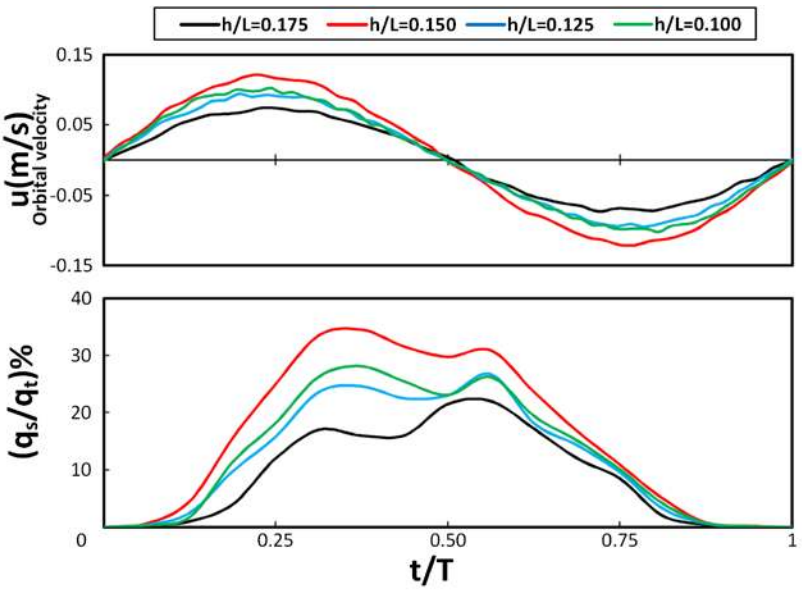

Figure 16: Horizontal orbital velocity and suspended load ratio during a wave period, horizontal orbital velocity (top), suspended load ratio (bottom)